Liquid Crystals
Publication details, including instructions for authors and subscription information:
http://www.informaworld.com/smpp/title~content=t713926090

Polymer-stabilized cholesteric liquid crystal microgratings: a comparison of polymer network formation and electro-optic properties for mesogenic and non-mesogenic monomers

Kyongok Kang; L. C. Chien; S. Sprunt

Online publication date: 11 November 2010

To cite this Article Kang, Kyongok , Chien, L. C. and Sprunt, S.(2002) 'Polymer-stabilized cholesteric liquid crystal microgratings: a comparison of polymer network formation and electro-optic properties for mesogenic and non-mesogenic monomers', Liquid Crystals, 29: 1, 9 — 18
To link to this Article: DOI: 10.1080/02678290110093732
URL: http://dx.doi.org/10.1080/02678290110093732

LIQUID CRYSTALS, 2002, VOL. 29, NO. 1, 9–18

Polymer-stabilized cholesteric liquid crystal micrograting: a comparison of polymer network formation and electro-optic properties for mesogenic and non-mesogenic monomers

KYONGOK KANG*, L. C. CHIEN† and S. SPRUNT

Department of Physics, Kent State University, Kent, OH 44242, USA
†Chemical Physics Interdisciplinary Program and Liquid Crystal Institute, Kent State University, Kent, OH 44242, USA

(*Received 31 May 2001; accepted 17 July 2001*)

Polymer-stabilized liquid crystal micrograting are made using a focused Gaussian UV laser beam to photopolymerize 3 wt % reactive monomer in a cholesteric liquid crystal host. In a typical case, round gratings of 300 μm diameter and 10 μm pitch are produced. The micrograting highlight interesting differences between mesogenic and non-mesogenic monomers in the assembly and spatial distribution of polymer networks formed in a cholesteric host. We also observe a corresponding variation in the electro-optical properties of the stabilized gratings. In the mesogenic case, the grating state of the liquid crystal is faithfully captured even for relatively short UV exposures and over regions only a few pitch lengths in size. These findings are consistent with phase separation of the mesogenic monomer into regular domains templated by periodic, macroscopic variations in orientational order of the host. This templating effect is significantly reduced in the non-mesogenic case.

1. Introduction

Electrically responsive diffraction gratings based on polymer-stabilized liquid crystals (PSLCs) are promising devices for electro-optic applications requiring low cost, low power, switchable diffracting elements [1–6]. A liquid crystal grating is conveniently formed from the natural variation in the local direction of the optic axis in a cholesteric. The orientation (and spatial homogeneity) of the grating vector may be manipulated by appropriate substrate treatments and applied electric or magnetic fields. In the latter case, an internal polymer network formed by UV photopolymerization of a minority (typically 3∼5 wt %) monomer component can be used to stabilize the grating state against removal of the field and mechanical shock. Thus, unlike planar gratings formed from pure cholesterics, the polymer-stabilized grating is able to operate repeatedly between a zero field 'on' and moderate field 'off' state without degradation due to reorientation of the helical axis and/or domain formation. Moreover, the network morphology can be significantly influenced by the liquid crystalline order [6–9] and, in turn, can modify the electro-optic response in useful ways—for example, by increasing the relaxation rate between the grating 'on' state and an 'off' state (where the optic axis is spatially uniform). Operating in the phase grating or Raman–Nath limit, cholesteric PSLC gratings are more flexible for beam steering applications than Bragg gratings; they also switch between states on relatively fast (ms) time scales‡.

In a recent report [6], the morphologies of polymer networks formed from mesogenic and non-mesogenic monomers in a cholesteric PSLC grating were compared, and a significant connection between morphology and electro-optic properties of the corresponding stabilized gratings was demonstrated. This work built on the earlier demonstration of an electrically switchable grating, but did not address the important underlying issue of the effect of monomer type on the stabilization process itself. Nor did it assess the more practical issue of the dependence of the electro-optic properties, for a given sample composition, on UV exposure conditions (power and time). In this paper, we focus on these issues, using micrograting textures (or 'microspots') formed with a focused UV laser beam as a new method to characterize the

*Author for correspondence; e-mail: kkang2@kent.edu

‡For practical applications, further studies will be needed to implement index matching between the polymer network and host liquid crystal, optimize network concentration for the best compromise between electro-optical properties and resistance to aging/temperature variation, utilize an asymmetric grating profile to produce a phase grating with single dominant diffraction spot for specified incidence, and minimize scattering losses (currently around 5% in the best case).

Liquid Crystals ISSN 0267-8292 print/ISSN 1366-5855 online © 2002 Taylor & Francis Ltd
http://www.tandf.co.uk/journals
DOI: 10.1080/02678290110093732

stabilization process, rate, and corresponding electro-optic properties of the gratings. When the UV wavelength is such that there is negligible absorption by the system, we find that efficient gratings are obtained using either a high power/short time or low power/long time exposure protocol, but that the diffraction patterns and dynamic responses differ significantly. We also observe that the stabilized microgratings in the non-mesogenic case develop more isotropically, both in shape and internal distribution of cured domains, while gratings based on the mesogenic monomer show a considerably more patterned, anisotropic growth.

2. Experimental approach

Our samples were prepared using a mixture of (by weight) 96.6% cholesteric liquid crystal (Merck E44 with 0.4% chiral dopant R-1011), 3% monomer, and 0.15% photointiator (Irgacure 651, Ciba Additives). The non-mesogenic monomer used was HDDA, which is isotropic at room temperature and above. The mesogenic monomer was RM257 (Merck), which has the phase sequence crystal–(70°C)–nematic–(120°C)–isotropic. Room temperature mixtures of these materials were loaded into commercial electro-optic cells (EHC, Japan), with a 10 μm spacing between anti-parallel rubbed polyimide alignment layers. The glass substrate surfaces were ITO coated to facilitate application of an electric field across the gap. When a $\sim$0.3 V μm^{-1}, 1 KHz square wave field is applied, the helical axis of the cholesteric reorients into the substrate plane perpendicular to the rub direction (which corresponds to the average alignment direction of the optic axis). This produces a planar grating (or 'fingerprint') texture, with the grating vector normal to the rub direction. The grating pitch is controlled by the chiral dopant concentration [2], and was chosen to be comparable to the sample thickness in order to minimize the number of grating defects [10].

The planar grating state was stabilized by photopolymerization of a polymer network. This was done using a 365 nm UV laser beam (Lexel model 95), focused to a $1/e^2$ spot size of $\sim$200 μm. The beam was polarized along the grating vector. In this case there is minimal diffraction of the UV wavefront, and thus minimal spreading of the beam. Both the exposure power (proportional to intensity since we always used the same beam spot size) and exposure time were varied, as described below. After sufficient time, the result of the UV exposure was the formation of a round grating with an overall diameter of a few hundred microns and a pitch (set by the dopant concentration) of approximately 10 μm (i.e. comparable to the cell thickness). Unlike polymer-stabilized cholesteric displays, these gratings are monostable textures. This is because the polymer network is *templated* by the grating texture [6], and so provides strong internal anchoring for the grating state. By contrast, the network in the display is not spatially patterned on either of the two operating states; the barrier between focal-conic (scattering) and planar states in this case is thus quite weak. Another crucial difference is the cell thickness to pitch ratio, which is very much larger than unity in the display and comparable to unity in the grating. This difference accounts for the presence of many randomly-oriented helical domains in the display, as compared with a monodomain (parallel to the substrate plane) for the grating.

Diffraction patterns and electro-optical properties of the gratings were measured with a HeNe laser beam focused to about half the spot size of the grating and polarized perpendicular to the grating vector. No analyser was used. The patterns were recorded on a CCD camera (Electrim model EDC-1000U), and the dynamic response of the gratings was measured using a photodiode (Thorlabs model PDA-50), amplifier circuit, and digital oscilloscope (Tektronix model TDS 430A).

3. Results and discussion

3.1. *Optical morphology of PSLC microgratings*

Figure 1 shows depolarized optical microscope images of typical microgratings stabilized by HDDA and RM257, using different exposure powers (0.11 and 17 mW respectively) and similar exposure times (7 and 15 s). The corresponding integrated energies required to cure comparably sized gratings are 0.78 and 2.5 mJ. The round, stabilized grating regions are surrounded by regions in which the helical axis of the cholesteric has reverted to its normal state (perpendicular to the plane of the figure or substrate plane) after removal of the applied field. There is a sharp transition between the two regions. Examination of the transition region reveals that in the RM257 case, the grating is stabilized all the way to the edge, whereas for HDDA there is a more random, isotropic layer around the edge. In both cases there are metastable filaments that remain from the field-distorted state, and pass between the spots and nearby spots (not shown) through unexposed regions of the sample. Figure 1 (*c*) demonstrates the feasibility of producing regular arrays of microgratings§. Shown is a portion of a square 20 by 20 array of HDDA microgratings each with 300 μm diameter and 10 μm micron optical pitch. (A larger number of defects are apparent

§The patterning of individual spots would be useful in applications requiring either highly localized gratings or discrete changes in diffractive properties ('stepped' format). To achieve such steps, one could use chiral reactive monomers, whereby the local twisting power (or pitch) of the stabilizing network could be tuned by a spatially varying exposure intensity or intensity gradient [11].

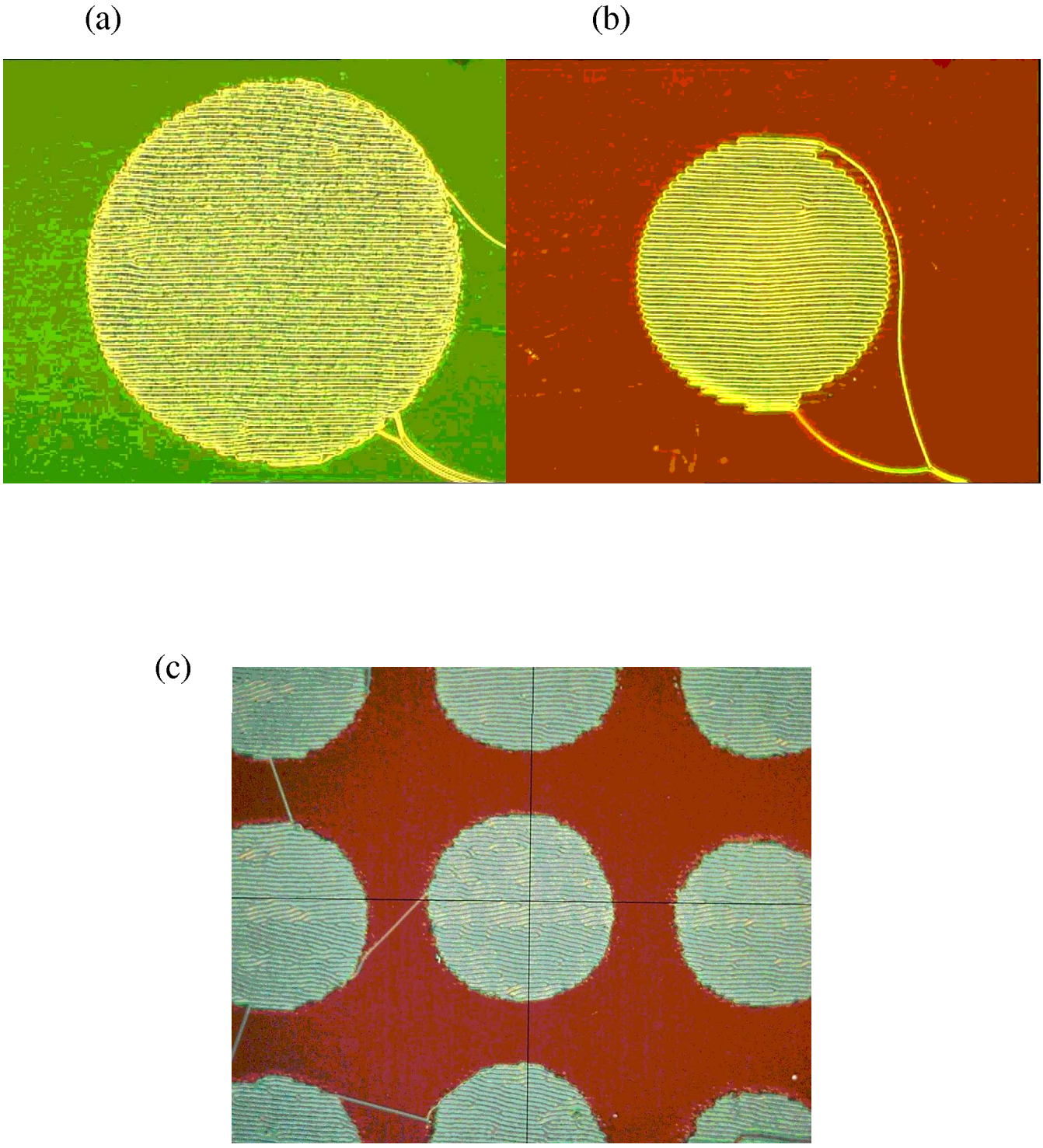

Figure 1. Optical textures of polymer-stabilized cholesteric microgratings. (*a*) A micrograting stabilized with HDDA after exposure to 0.78 mJ of 365 nm UV laser radiation; the spot diameter is 400 µm. (*b*) A 300 µm grating stabilized with RM257 after exposure to 2.5 mJ. (*c*) A portion of a 20 by 20 square array of 300 µm HDDA gratings.

in the gratings in the array because the applied field strength was not optimized in this case.). In figures 1 (*a*) and 1 (*b*), the colours transmitted through the regions of normal state cholesteric differ. This is probably because the ratio of chiral dopant to mesogen in RM257 mixtures is slightly lower than in HDDA mixtures, resulting in a

somewhat longer helical pitch for the RM257 case. Also, for the same initial mixture, we observed different background colours for a dense array of microspots, figure 1 (*c*), and a single isolated spot, figure 1 (*a*). At present we cannot explain this difference.

A closer look at the early stage growth and development of stabilized micrograting highlights a striking difference between the formation process of HDDA and RM257 networks in the same cholesteric host. In each column of figure 2, identical samples containing HDDA or RM257 were exposed at the same UV power spot size, but for different times. After exposure the unstabilized region was then allowed to relax back to the normal state, which produces the featureless background in each of the figures. In both cases, stabilization proceeds outwards from the centre of the exposed region, which corresponds to the point of maximum power in the Gaussian beam profile. At an early stage, (*a*) and (*c*), the regions where the distorted state of the liquid crystal has been partially stabilized reveal that the HDDA network grows as thin filaments, which are oriented in a nearly random fashion with respect to the wave vector of the grating state (vertical in all the figures). The network then fills in at later times, (*e*), stabilizing a relatively uniform grating state of the liquid crystal only when relatively dense network occupies almost the full exposure area. During the network development, the perimeter of the stabilized central region continues to show the characteristic early stage of random filaments.

In contrast, the regions stabilized by the RM257 network, figures 2 (*b*), 2 (*d*) and 2 (*f*), are highly patterned, even at early times, by the grating state of the liquid crystal. Note in (*b*) that the grating texture of the liquid crystal can be efficiently captured even in a relatively small region at the centre of the exposure area. Before it completely fills the circular exposure area, the shape of the RM257 stabilized domain also appears notably elongated along the grating vector, (*b*) and (*d*). We confirmed that this shape anisotropy is independent of UV polarization, and so is not strictly an effect due to internal diffraction or beam spreading associated with the liquid crystal grating. Finally, the periphery of the RM257 stabilized regions is quite different from the HDDA case, compare (*c*) and (*d*), or (*e*) and (*f*). For RM257, there is a sharp transition from full stabilization (or nearly complete network formation) to a very weakly stabilized surrounding region. The surrounding texture clearly reflects the templating effect of the grating on the network structure, a feature not observed for HDDA. The contrasting textures at the periphery are shown in figure 3 at an additional 6.4X magnification.

The differences observed in the stabilization of grating states between RM257 and HDDA can be explained by considering that, prior to polymerization, the mesogenic monomer RM257 phase separates into periodically spaced domains commensurate with the grating pitch. Recent simulations of the director distribution in the grating state yield a structure consisting of periodic regions of π-twist separated by narrow walls of uniformly oriented director that run between opposite substrates in a zigzag fashion [11]. SEM images of the final network structure strongly suggest that the mesogenic monomer is initially concentrated near the boundaries of the more uniform regions and that it mimics the director orientation of the host [12]. An anisotropic initial monomer distribution would account for the patterning observed even in weakly exposed, partially stabilized peripheral regions surrounding the central stabilized spot in figures 2 (*b*), 2 (*d*) and 2 (*f*). On the other hand, one expects the non-mesogenic HDDA monomer to be less influenced by the orientational order of the host, and therefore to be decoupled from the host director, and perhaps more isotropically distributed in space prior to polymerization. Then the HDDA network is less efficiently patterned by the host, and therefore less effective at low exposure levels in accurately capturing the grating state. Furthermore, if the RM257 monomers are oriented along the liquid crystal director (average long molecular axis), they will diffuse anisotropically, with a larger diffusion constant parallel to the director. From the elongation of the stabilized region along the grating axis in figures 2 (*d*) and 2 (*f*), we then surmise that the component of the RM257 long axis lying in the substrate plane points, on average, along the grating vector. This is consistent with recent SEM images [6] of the RM257 network structure, which show a zigzag pattern of polymer walls running between top and bottom substrates and forming a corrugated structure. The walls consist of dense fibrils whose average orientation in the face of the walls is observed to be parallel to the grating vector, indicating an 'easy' direction for monomer diffusion.

Data for the increase in the average radius of the stabilized region with exposure time (figure 4) also show a marked difference between the two monomers, and are consistent with a bulkier, more highly phase-separated RM257 network. These data were taken for comparable UV powers (0.01 mW), and thus the total energy on the horizontal axis is proportional to exposure time. The final diameter of the stabilized spots is 300 and 270 μm for HDDA and RM257, respectively. The resulting curves shown in figure 4 have the same shape, but are substantially shifted on the horizontal axis. The growth of the stabilized grating region for RM257 with exposure energy (or equivalently time, for our data) is about 6.5 times slower than for HDDA. One natural explanation of this difference is that the larger RM257 molecule diffuses more slowly than HDDA in the host. We roughly estimate this effect by considering the monomer to be a

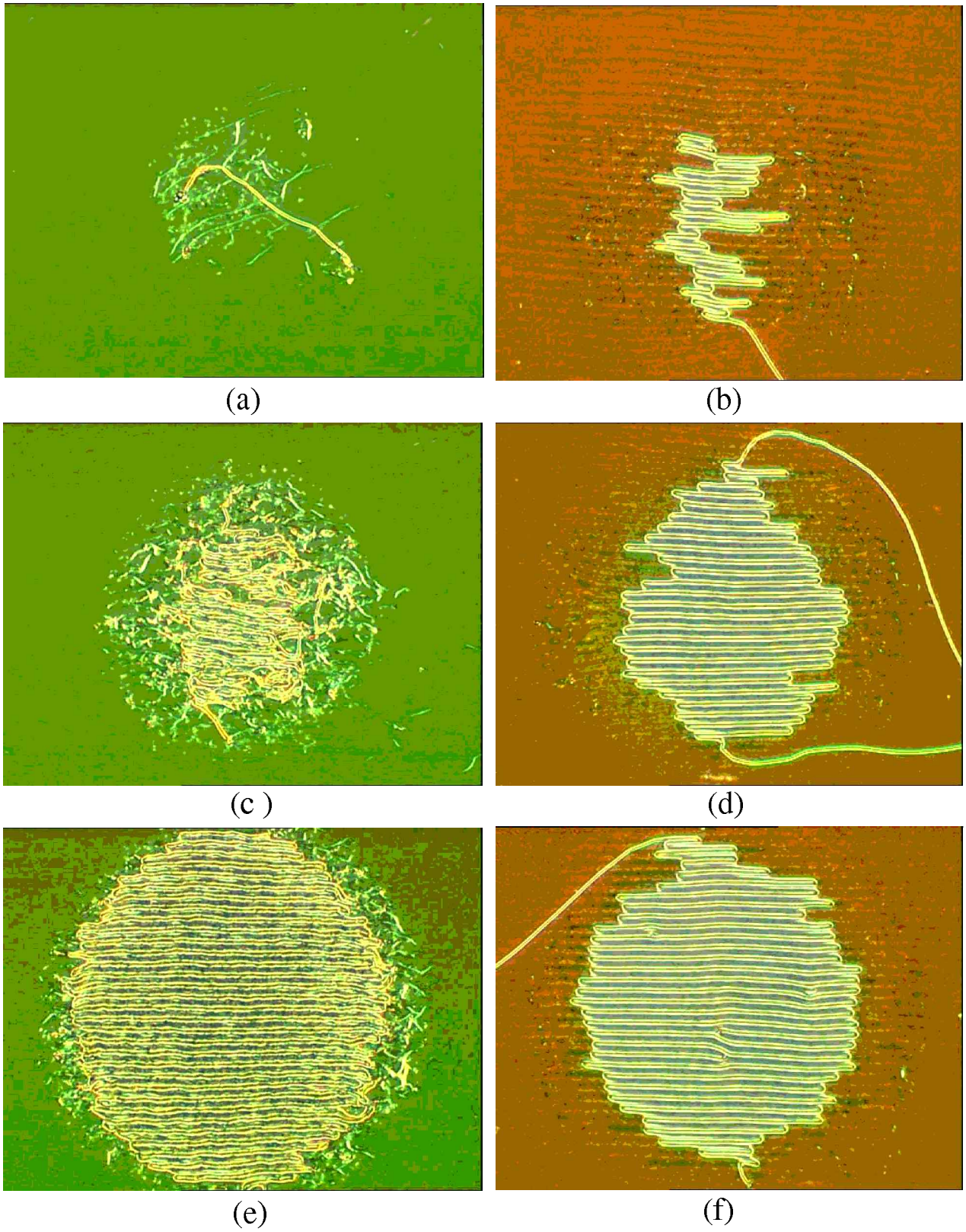

Figure 2. Micrograting stabilization as a function of UV exposure time for a fixed UV spot size. (*a*), (*c*), (*e*): HDDA-based gratings after exposure to 0.06, 0.09, and 0.19 mJ, respectively, at 0.03 mW intensity. (*b*), (*d*), (*f*): RM257-based gratings after exposure to 0.94, 1.21, and 1.34 mJ, respectively, at 0.13 mW intensity.

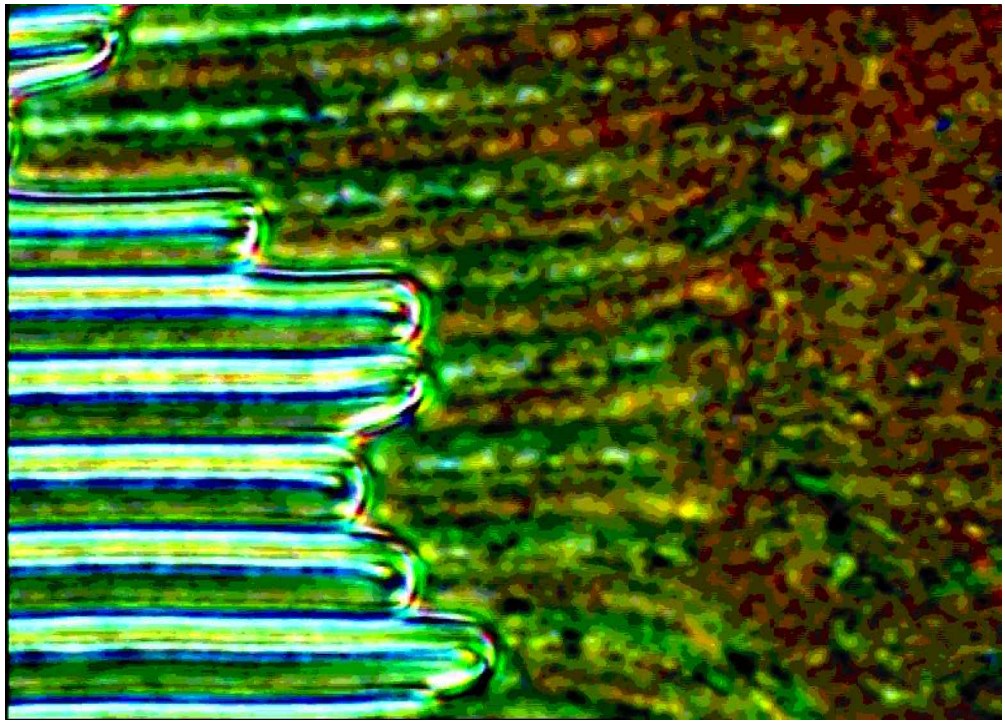

(a)

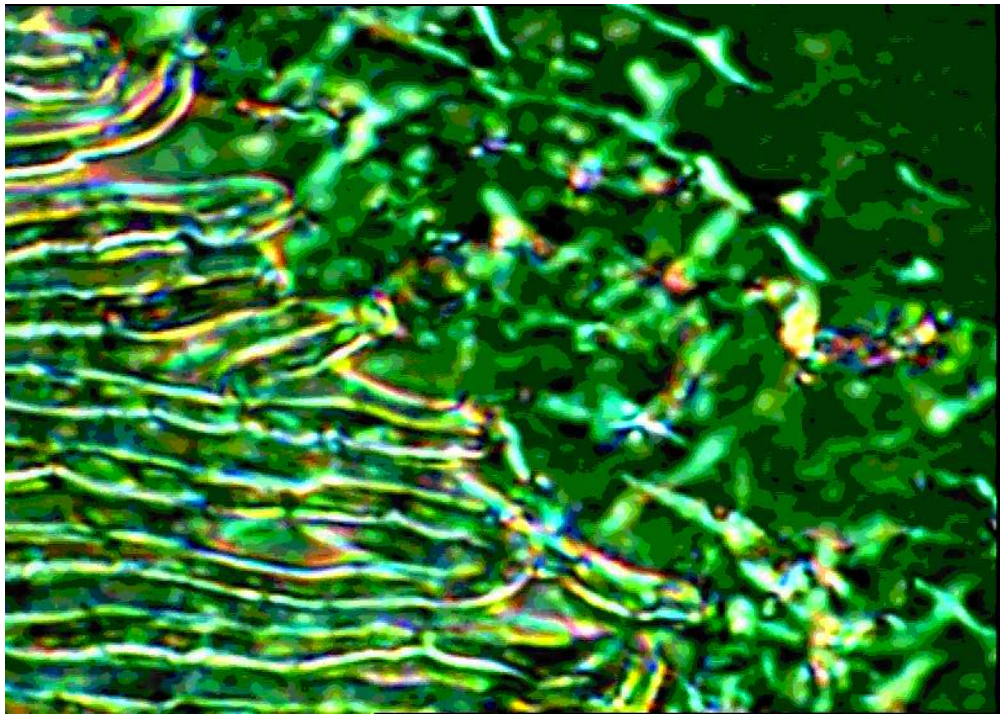

(b)

Figure 3. Detail of edge region of (*a*) RM257 and (*b*) HDDA micrograting.

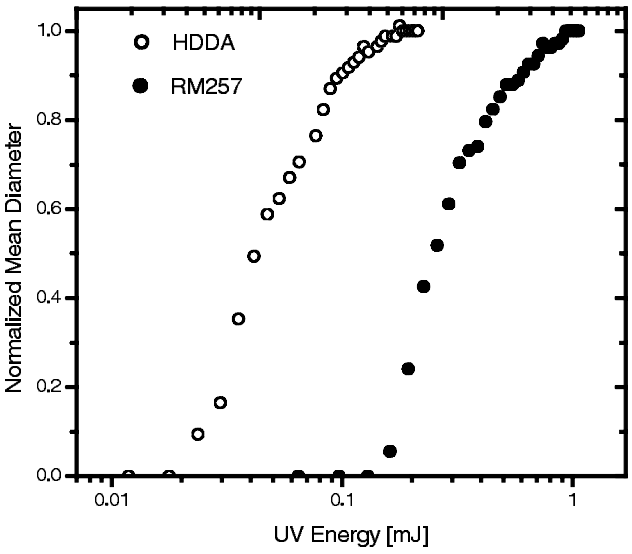

Figure 4. Stabilized grating size as a function of applied UV energy for HDDA and RM257-based gratings.

rigid rod, with translational diffusion constant $D \sim L^{-1}$, where L is the rod length [13]. Since the diameters of the molecules are comparable, we can assume L scales with the molecular weight. Then we find $D_{\mathrm{HDDA}}/D_{\mathrm{RM257}} \sim 2.5$. This is less than the observed factor of 6.5. To account for the difference, we can postulate that templating by the host significantly inhibits the freedom of the mesogenic monomer to explore orientational phase space, slowing the development of the network.

3.2. *Electro-optic properties of PSLC micrograting*s

We now turn to the electro-optic properties of the micrograting. In figures 5 and 6, we display diffraction patterns obtained in transmission from a normally incident HeNe laser beam on micrograting stabilized with HDDA and RM257 networks under various UV exposure conditions. The laser was polarized perpendicular to the grating axis and focused to a 100 μm spot; no analyzer was used. For HDDA gratings, the exposure conditions were 0.02 mW for 40 s ['low power/shorter time', figure 5 (*a*)], 0.02 mW for 1200 s ['low power/longer time', figure 5 (*b*)], and 2 mW for 8 s ['high power/shorter time', figure 5 (*c*)]. The corresponding conditions for RM257 gratings were 0.63 mW for 20 s [figure 6 (*a*)], 0.63 mW for 120 s [figure 6 (*b*)], and 10 mW for 10 s [figure 6 (*c*)]. The diffraction patterns were taken using square waveforms of an applied voltage, with the peak value optimized for maximum diffracted intensity. In figures 5 (*d*) and 6 (*d*), we also show an 'off' state for micrograting stabilized under the high power/shorter time condition.

Let us first compare the effect of low and high exposure powers at the shorter exposure times [panels (*a*) and (*c*) in figures 5 and 6]. Panels (*a*) reveal that RM257 networks stabilize more efficient gratings than HDDA networks for the low powers, shorter time exposures. This is consistent with figure 2, where RM257 stabilizes better (though smaller) replicas of the liquid crystal grating for a given exposure energy (and fixed exposure area). At the higher exposure power [panels (*c*) in figures 5 and 6], both monomers produce efficient gratings. When optimized under an applied field of 0.55 V μm^{-1} at 1 kHz, the HDDA grating shows strong first order diffraction, corresponding to the optical period observed in figure 1, whereas the most efficient RM257 grating (at 0.35 V μm^{-1}) exhibits nearly equal diffraction into first and second orders. Increasing exposure time at the lower UV power [panels (*b*) in figures 5 and 6] reveals a somewhat different trend. In this case the most efficient RM257 grating (at 0.40 V μm^{-1}) produces nearly pure second order diffraction, while the optimized HDDA grating (at 0.30 V μm^{-1}) now shows equivalent first and second orders. Figures for single-order diffracted intensity divided by total transmitted intensity (total diffracted plus undiffracted beam intensity) are 93% [HDDA, panel (*b*) in figure 5] and 96% [RM257, panel (*b*) in figure 6]. (The transmitted intensity does not include scattering, which reduce these figures to 85% and 90%, nor have we included ~10% reflection losses.)

The diffraction patterns reveal a greater tendency for RM257-based micrograting to produce substantial diffraction at twice the wave vector of the cholesteric helix—i.e. second order diffraction—as compared with the more prominent first order diffraction in HDDA-based gratings. The two sources of optical contrast in the sample—spatial variation of the liquid crystal director arising from the cholesteric structure and alternation of polymer-rich and polymer poor regions—have the same optical period, and thus do not by themselves produce a strong second order peak. However, we can again explain our observation by assuming stronger patterning of the RM257 network by the host. A tendency for the RM257 monomer to order locally along the host director leads to a final network morphology consisting of periodic, close packed arrays of fibrils [6]. Such a morphology produces a high network surface to volume ratio (in the polymer rich regions). If the fibrils are uniaxially aligned [6], one has strong homogeneous anchoring conditions on the liquid crystal host. Then, at the interfaces to the network-rich domains, the liquid crystal strongly resists rotation by the applied field. In contrast the optic axis at the centre of liquid crystal-rich regions responds more readily to low fields. Thus there is a likelihood of achieving an index match between the centres of the polymer-rich and liquid crystal-rich

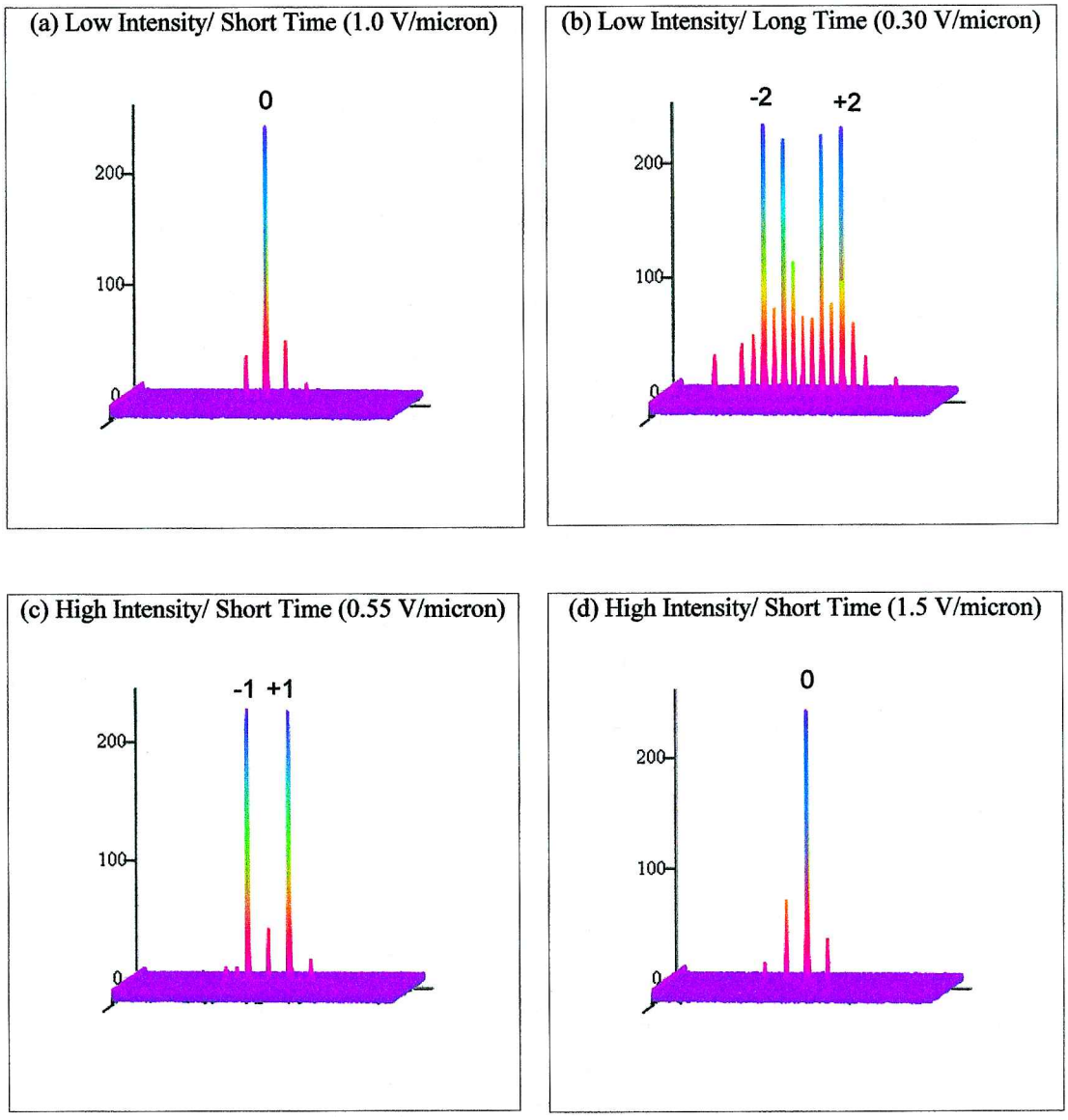

Figure 5. Foward diffraction patterns for an HDDA-based micrograting for different UV cure conditions. In (*a*)–(*c*), the peak value of the applied voltage was optimized for maximum diffracted intensity. Panel (*d*) displays an 'off' state (minimum diffraction). The integers 0, ± 1, ± 2 label zeroth, first, and second diffraction peaks, respectively. First order corresponds to a diffraction angle of 7.2°.

regions at low fields. This scenario would introduce a strong second harmonic to the grating profile (i.e. twice the original optical period), and explain the observed strong second order peak. Alternatively, if the morphology for HDDA is not so closely organized around the host director orientation—so that there is no preferred orientation embedded in the network and no templated fibril structure—there would be less chance for doubling the grating period by the mechanism described.

We have also studied selected features in the dynamic response of the HDDA-based microgratings. We first consider the optical response of the zero order transmitted beam when the grating is switched from its 'off' state (maximum zero order transmission) to its 'on' state (minimum forward transmission) by reducing the applied field. There will in general be two coupled components to the response: one due to the 'fast' relaxation of the liquid crystal and a second due to the 'slow' relaxation of the polymer network. Figure 7 (top plot) shows that, for comparable total UV energies, gratings exposed for longer times at low power relax more rapidly (with weaker polymer component) than the same initial mixture exposed at high power for short time. Also the turn-off voltage in the low power/longer time case is significantly

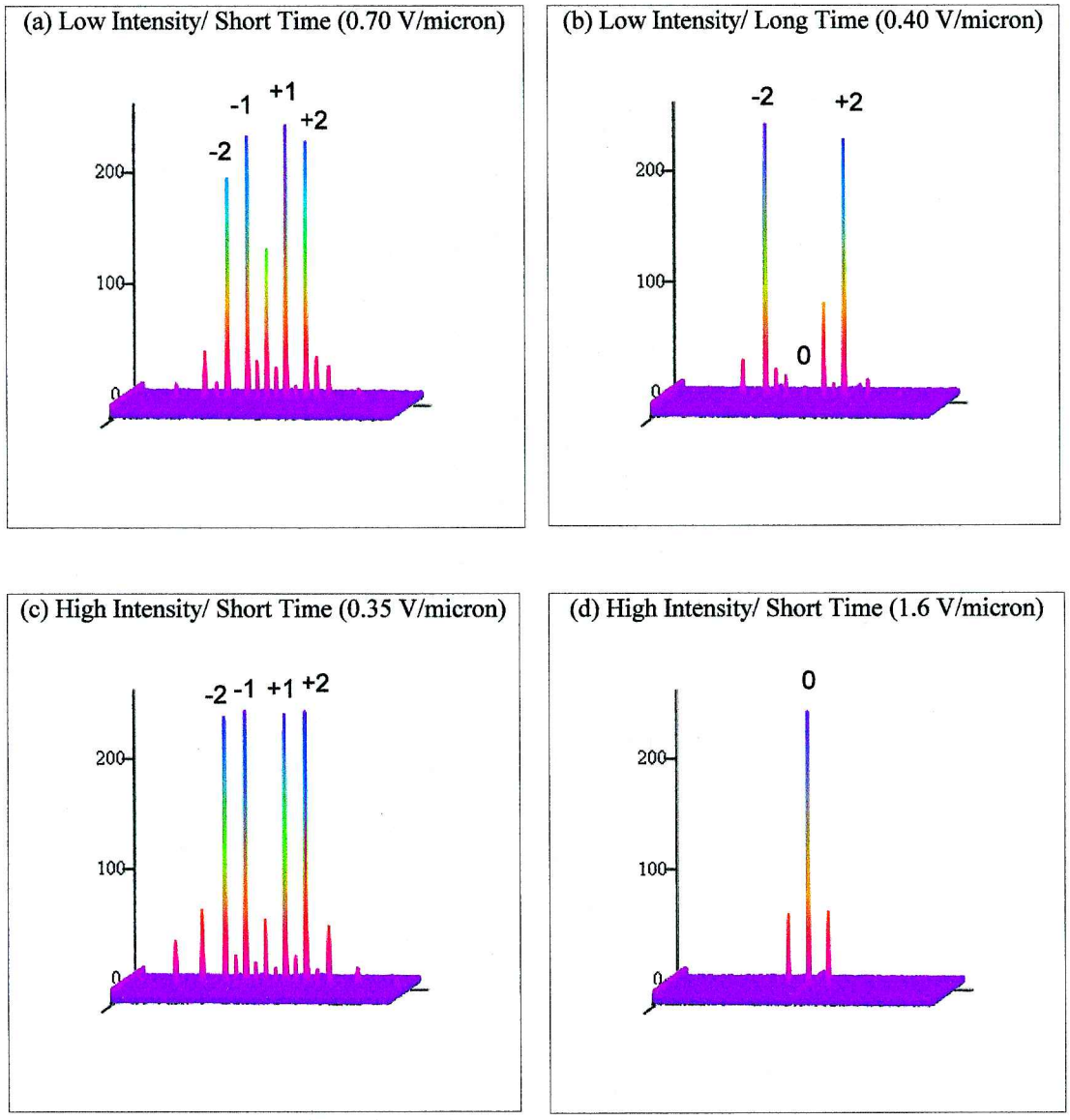

Figure 6. Forward diffraction patterns for an RM257-based micrograting for different UV cure conditions (details in text). As in figure 5, panel (*d*) displays an 'off' state.

lower (approximately a factor of 2). Figure 7 also compares the turn off dynamics of the zero order (applied field switched *off*) (centre plot) and first order diffraction peak (applied field switched *on*) (bottom plot) in the grating formed under low power/longer time exposure conditions. When the optical response is driven by a field of 0.30 $V\mu m^{-1}$, the response time is, as expected, shorter (0.9 vs. 4.0 ms at the $1/e$ point in the transition).

4. Conclusion

In this paper we have illustrated how stabilized microdomains of the 'fingerprint' texture of a cholesteric reveal important differences in the formation of stabilizing polymer networks based on mesogenic and non-mesogenic monomers. We have also demonstrated how the electro-optic properties of the diffraction gratings produced by these microdomains depend on the monomer type and on the conditions of UV exposure used in photostabilization. Single and arrays of microgratings are easily made, and relatively sharp interfaces are achieved between the gratings and the surrounding undistorted state of the liquid crystal.

This work was supported by the Office of Naval Research under grant no. N00014-99-1-0899 and by ALCOM/NSF under grant no. DMR-8920147.

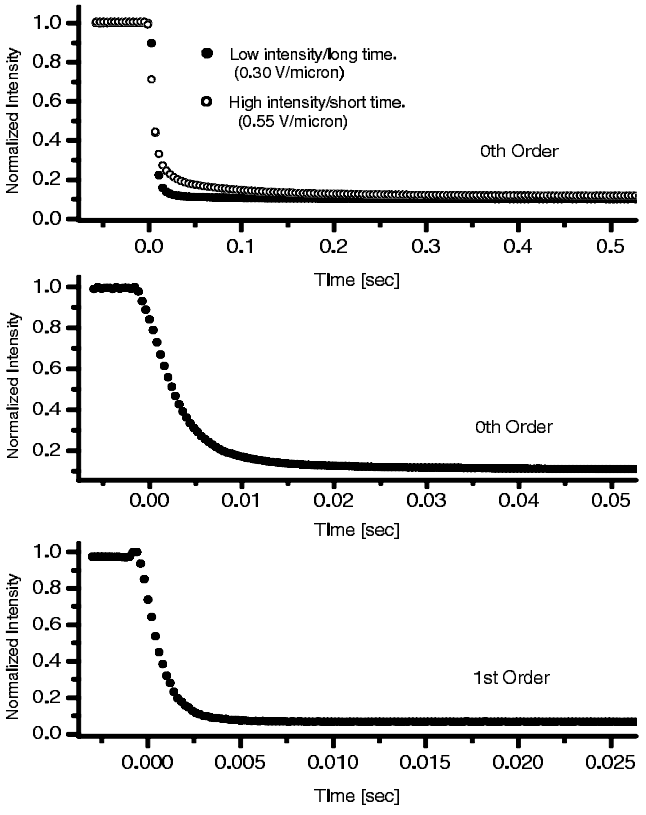

Figure 7. Dynamic response of HDDA-based microgratings for two different UV cure conditions.

References

[1] Scffer, B. H., Margerum, J. D., Lacker, A. M., and Boswell, D., 1981, *Mol. Cryst. liq. Cryst.*, **70,** 145.

[2] Lee, S. N., Chien, L. C., and Sprunt, S., 1998, *Appl. Phys. Lett.*, **72,** 885.

[3] Sutherland, R. L., Tongdigla, V. P., and Natarajan, L. V., 1994, *Appl. Phys. Lett.*, **64,** 1074.

[4] Subacious, D., Bos, P. J., and Lavrentovich, O. D., 1997, *Appl. Phys. Lett.*, **71,** 1350.

[5] Subacious, D., Shiyanovschi, S. V., Bos, P. J., and Lavrentovich, O. D., 1997, *Appl. Phys. Lett.*, **71,** 3323.

[6] Kang, S. W., Sprunt, S., and Chien, L. C., 2000, *Appl. Phys. Lett.*, **76,** 3516.

[7] Zhang, J., Caren, C. R., Palmer, S., and Sponsler, M. B., 1994, *J. Am. chem. Soc.*, **116,** 7055.

[8] Fuh, A. Y.-G., Ko, T.-C., Tsai, M.-S., Huang, C.-Y., and Chien, L. C., 1998, *J. appl. Phys.*, **83,** 679; Dierking, I., Kosbar, L., Lowe, A., and Held, G., 1998, *Liq. Cryst.*, **24,** 397.

[9] Lee, S. N., Sprunt, S., and Chien, L. C., 2001, *Liq. Cryst.*, **28,** 637.

[10] DeGennes, P. G., and Prost, J., 1993, *The Physics of Liquid Crystals*, 2nd Edn (Oxford: Clarendon Press), p. 283.

[11] See for example, Broer, D. J., Lub, J., and Mol, G. N., 1995, *Nature*, **378,** 467.

[12] Kang, S. W., Chien, L. C., and Sprunt, S., unpublished results.

[13] De Gennes, P. G., 1990, *Introduction to Polymer Dynamics* (Cambridge: Cambridge University Press), pp. 10–12.